Geophysical Journal International

Geophys. J. Int. (2012) **188,** 1012–1024 doi: 10.1111/j.1365-246X.2011.05310.x

An investigation into the debris flow induced by Typhoon Morakot in the Siaolin Area, Southern Taiwan, using the electrical resistivity imaging method

Ping-Yu Chang,[1] Chien-chih Chen,[2] Shu-Kai Chang,[1] Tzu-Bin Wang,[2] Chien-Ying Wang[2] and Shu-Kun Hsu[2]

[1] *Institute of Applied Geosciences, National Taiwan Ocean University, No.* 2*, Beining Rd., Keelung,* 20224 *Taiwan, ROC*
[2] *Department of Earth Sciences and Institute of Geophysics, National Central University, No.* 300*, Jhongda Rd., Jhongli,* 32001 *Taiwan, ROC.*
E-mail: chencc@ncu.edu.tw

Accepted 2011 November 17. Received 2011 November 10; in original form 2010 June 11

SUMMARY

A massive debris flow induced by Typhoon Morakot buried the southern Taiwan village of Siaolin in Jiaxian township and caused the deaths of an estimated 474 people. To reconstruct the mechanisms triggering the tragic debris flow, researchers must identify the subsurface structures of the debris-flow sediments. For this purpose, we conducted 2-D, electrical resistivity imaging (ERI) surveys along networked lines where the village once stood. With the imaging results, we identified three layers, including the basement of Yenshuikeng Shale, the newly accumulated debris-flow deposits; and the old fluvial deposits amid the basement and the debris-flow sediments. According to the resistivity results, the bottom of the debris-flow deposits is under the old ground surface in three eroded areas, C1, C2 and C3. Resistivity anomalies in the debris-flow sediment layer are well correlated with the locations of houses and the major roads in the piling area (P1) and the eroded area (C2). Hence these findings indicate that the basal erosion of the debris flow may have occurred in areas C1, C2 and C3 since a specific mass movement may undercut into the basal sediments or rocks and forms a filled trench in its basement. These eroded areas may be related to different events of mass movements due to their different orientations of basal erosion. From the resistivity image we estimated the volume of debris flow is underestimated for about 24.5 per cent to the estimated volume of the debris flow from digital terrain models (DTMs) in the study area. We conclude that the volume of a debris flow may be underestimated because of the basal erosion if only data from DTMs are used for its calculations and present new means for its correction by combining DTM and ERI results.

Key words: Electrical properties; Magnetic anomalies: modelling and interpretation; Geomorphology; Hydrogeophysics; Controlled source seismology; Asia.

INTRODUCTION

Typhoon Morakot, a category-2 hurricane, made its landfall in central Taiwan on 2009 August 7, and in 72 hours unleashed total rainfall of more than 2700 mm on southern Taiwan. The record-breaking rainfall induced debris flows that impacted many mountainous areas along the Cishan and the Laonong rivers in southern Taiwan. Among the impacted areas was the village of Siaolin in Jiaxian township. This village was the site of a giant debris flow that buried almost the entire village and caused the deaths of an estimated 474 people, including missing people who are presumed dead (Lee *et al*. 2009; Chen 2010).

To better understand the mechanisms and processes that triggered the giant debris flow, it is important to illustrate the distribution patterns of the debris-flow sediments. Although researchers have estimated the distribution of the debris flow by comparing before-and-after digital terrain models (DTMs) of Typhoon Morakot (e.g. Lee *et al*. 2009; Tang *et al*. 2009; Kuo *et al*. 2011), the resulting estimates rest on the two-fold assumption that only an accumulation of sediments took place in the event and that the previous topography in the Siaolin area remained undamaged during the debris flow. However, previous studies show that the basal erosion of the pre-existing ground surface may occur in the bottom boundaries of a sliding or flowing mass (e.g. Corominas 1995). The basal erosion process makes the volume estimations by DTMs may be erroneous and need to be verified with nondestructive methods. For this purpose, we conducted vast 2-D electrical resistivity imaging (ERI) surveys to resolve the spatial distribution of the debris-flow sediments in the Siaolin area.

Siaolin village was originally located on a fluvial river terrace that is approximately 3–5 m higher than the adjacent Cishan River (Fig. 1). Because the fluvial sediments have undergone natural

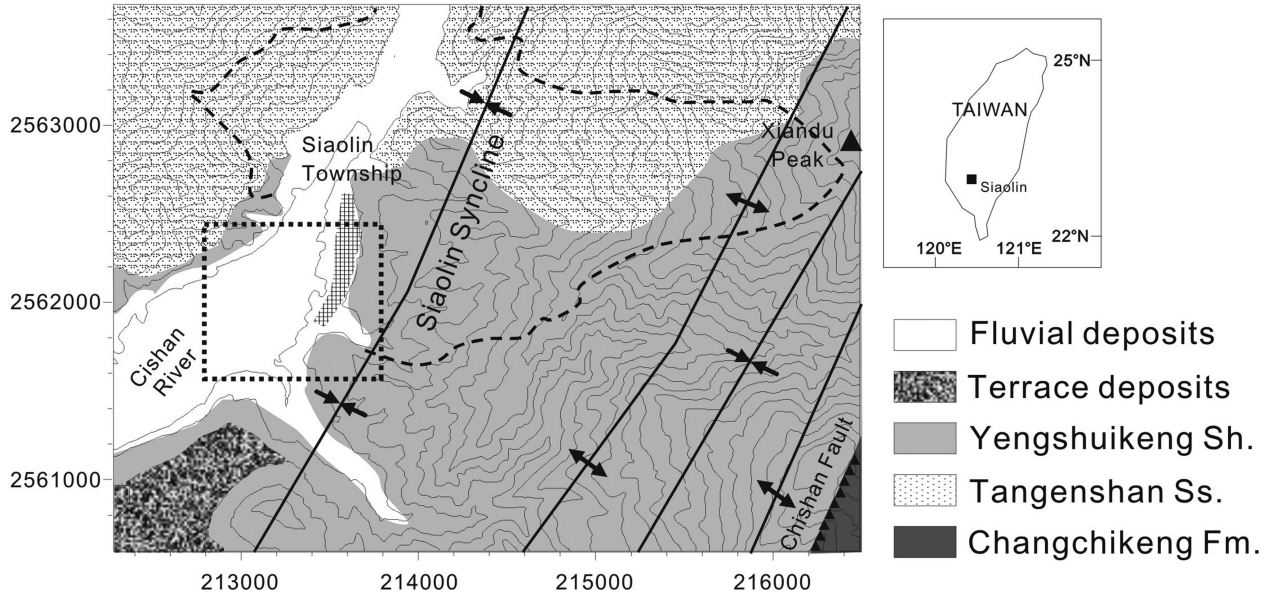

Figure 1. A geological map of the Siaolin area. Dashed lines indicate the borders of the debris flow induced by Typhoon Morakot. Light dotted lines indicate the resistivity survey area indicated in Fig. 2.

compaction for a long time, one would expect that the recent debris flow (with its loose interior and unsaturated textures) would exhibit a higher resistivity due to its higher porosity and its larger proportion of air-filled pores than would have been present in the 'old' fluvial sediments. This premise strengthens the argument that it is reasonable to illustrate the debris-flow distribution with resistivity distribution images. With the ERI results, we identified three layers including the basement of Yenshuikeng Shale (Fig. 1), the debris-flow sediment, and the old fluvial deposits with resistivity amid the basement and the debris flow. Also we examined the possible error and resolution of the ERI results with forward simulation methods using different three-layer geological models. We found that one would expect depth estimation errors within 1 m for the models with debris flow bottoms less than 8 m.

In addition to the resistivity surveys, we carried out magnetic surveys, horizontal-loop electromagnetic (HLEM) surveys, and shallow seismic refraction surveys in the area to uncover as much subsurface information as possible while accounting for excavation restrictions requested by the victims' families. We compared the resistivity anomalies representing possible building relics and the depths of the debris-flow sediments to data from the landscapes that existed before Typhoon Morakot. Our goal was to characterize possible sedimentary events on the basis of geophysical explorations. Results obtained from geophysical surveys suggest that the basal erosion of the debris flow may have occurred in three areas that may be related to three different landslide events. The findings also suggest that one may underestimate the volume of a debris flow if the basal erosion process occurs and only data from DTMs are used for the volume calculations.

The content of this paper is arranged in the following order: First, we introduce the geological settings and our survey plan in the area. Then we present the results of 2-D resistivity surveys, analyse the regional resistivity structures, and compare the explanation of resistivity results to the magnetic, shallow seismic refraction and HLEM explanations. In the discussion section, we explore the resolution of our ERI survey configurations with the forward modelling method. Finally, the spatial relationships between the debris-flow basement identified from the resistivity results and the DTM erosion calculations are investigated and discussed to analyse possible landslide events induced by the Morakot Typhoon in the Siaolin area.

GEOLOGICAL SETTING

Fig. 1 shows the geological setting of the area of Siaolin village (edited from Lee *et al*. 2009). The village is located on a narrow Holocene fluvial plain in the Cishan River Valley. The basement of the fluvial deposits is the Pliocene Yenshuikeng Formation, which consists of thick shale with a thin sandstone lens. Shale has cropped out along the eastern border of the village and at the river channel. The Tangenshan Sandstone underlies the Yenshuikeng Formation, and the sandstone can be observed at the west bank of the Cishan River. The Siaolin Syncline passes through an area east of the village. Both the Yenshuikeng Formation and the Tangenshan Sandstone strike to the northeast and dip toward the east at the western limb of the syncline near the village. At the eastern limb of the Siaolin Syncline, the Yenshuikeng Formation and the Tangenshan Sandstone strike northwest and dip toward the west. The Chishan Fault, a major fault structure in the area, is located approximately 3 km southeast of Siaolin village and separates the Yenshuikeng Formation from the Changchikeng Formation.

The sources of the debris flow are located close to the Xiandu Peak, which is northeast of the village and has an elevation of 1380 m above sea level. A 590-m-high hill is located on the northeast side of Siaolin village in the path of the debris flow. After Typhoon Morakot, the elevations of Xiandu Peak and the 590-m-high hill were reduced to approximately 800 m and 570 m, respectively. During Typhoon Morakot, most of the village was buried under debris-flow sediments with thicknesses of 6 to over 30 m. The northern part of the village is now covered with very thick debris-flow sediments that have formed a small hill. As a result, our study area is located mainly in the southern part of the village.

SURVEY PLANS AND IMAGING PROCESS

Electrical-resistivity surveys employ a direct current or an alternating current of very low frequency and explore the distribution

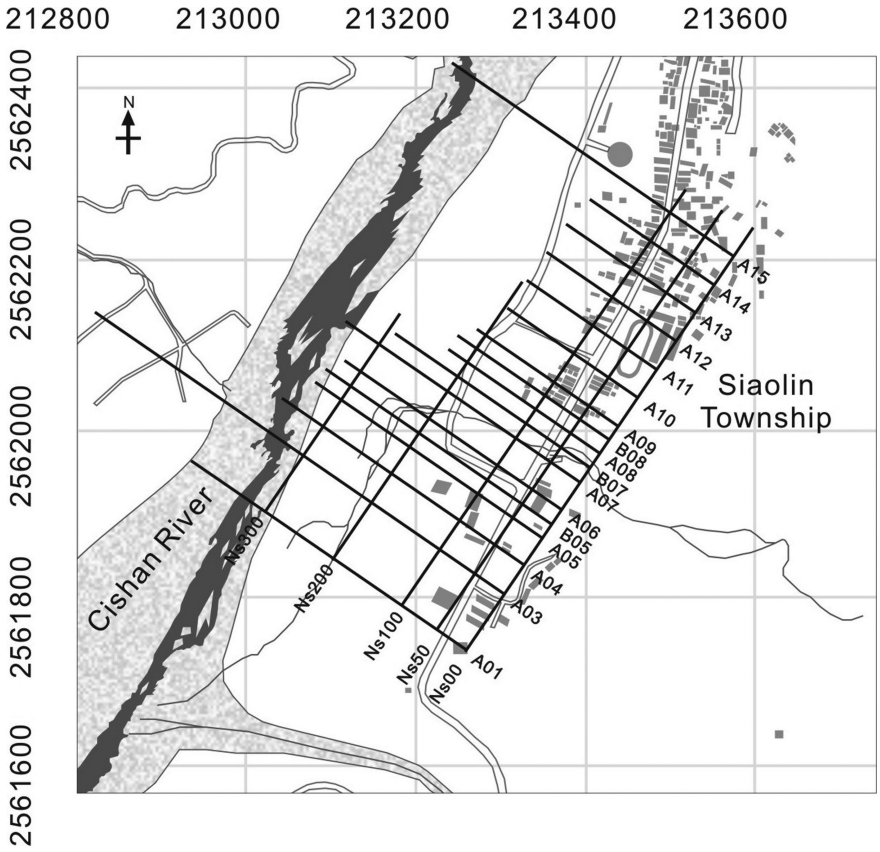

Figure 2. A map of Siaolin village outlines and the resistivity survey lines. The labels A1–A15 and NS00–NS300 indicate the locations of survey lines.

of apparent resistivity in the ground by measuring the variation of spatial potential fields. The image that shows the resistivity model in the subsurface can be obtained after one applies proper techniques for inverting the apparent resistivity measurements to a resistivity model. 2-D surface-based resistivity-imaging surveys have been widely used in various shallow subsurface explorations (e.g. Daily & Ramirez 1992; Griffith & Barker 1993; Cassiani *et al*. 2006; Hsu *et al*. 2010). In some cases, the 2-D sections are combined to form reasonably accurate images of 3-D structures (e.g. Dahlin & Loke 1997; Bernstone *et al*. 1997). The 2-D and 3-D resistivity-imaging techniques have been increasingly used to explore potentially unstable slopes because the techniques provide accurate information about the distributions and physical properties of geological structures (De Vita *et al*. 2006; Friedel *et al*. 2006; Green *et al*. 2006). In addition, the electrical properties of soils and rocks depend mainly on water content (Telford *et al*. 1986), which critically influences slope stability (Piegari *et al*. 2009).

We first tested different electrical array configurations (including Wenner, dipole–dipole and pole–pole arrays) on a survey line in the Siaolin area. Results from the pilot test showed that the dipole–dipole and Wenner measurements often revealed small and sporadic near-surface conductive objects from building relics off the survey lines. Data strongly saturated with these nearby-disturbance responses exhibited a trapezoid-shape structure in the Wenner and dipole–dipole pseudo-section and made the measurements unable to correctly resolve the deeper geological structures. Since in our pilot test the pole–pole measurement yields less responses to the off-line near surface disturbances, we chose to conduct networked 2-D pole–pole resistivity surveys along 18 parallel northwest–southeast (NW–SE) trending lines (A01, A02, A03, A04, A05, A06, A07, A08, A09, A10, A11, A12, A13, A14, A15, B05, B07 and B08) as well as five parallel northeast–southwest (NE–SW) trending lines (NS00, NS50, NS100, NS200 and NS300).

Fig. 2 shows the map of the resistivity-survey lines projected onto a geographic map of Siaolin village before Typhoon Morakot. The NE–SW-trending survey lines are parallel to the major pre-typhoon thoroughfare in Siaolin village, and the NW–SE-trending survey lines roughly traverse the thoroughfare. We hoped that the layout of electrode arrays along these two different orientations would enable us to investigate the changes characterizing the debris-flow subsurface structures in detail. The distances separating the parallel lines ranged from 20 to 40 m for the NW–SE lines and from 50 to 100 m for the NE–SW lines. We relied on a roll-along pole–pole method for the resistivity surveys with an electrode spacing of 1 m. The OYO McOHM Profiler-4 system with two 64-channel scanners and two passive cables was used for the electrical-resistivity survey. Two electrodes (the sink and the potential-reference electrodes) were placed approximately 2000 m away, which was a distance of more than 10 times the spreading length of each electrode cable. Because the designated survey area was covered by the debris flow (with estimated thicknesses of 6 to 20 m), the data were collected up to 40 levels; that is, the maximum distance between the source electrode and the potential electrode was 40 times the electrode spacing. On the survey lines, both the starting-electrode positions (0 m) and the electrode positions at 50-m intervals (i.e. 50 m, 100 m, 150 m and so on) were marked in the field with labels and recorded with a GPS for tracking of the survey geometries. For the roll-along pole–pole surveys, we utilized the measurement by moving half of the electrodes to the prospective locations along the survey lines.

The resistivity data were inverted with the EarthImager^{TM} 2-D software (AGI 2009). The software employs finite element forward solutions and an iterative conjugate gradient inversion scheme,

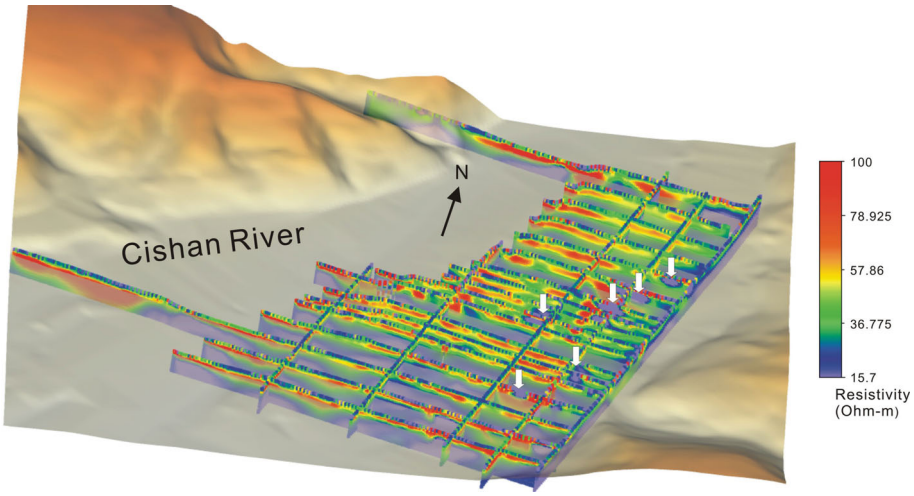

Figure 3. The fence diagram constructed with the inverted-resistivity profiles. Topography shown here indicates the ground surface before Typhoon Morakot.

described in more detail by Yang (1999), to estimate the subsurface resistivity structure. In analogy to Constable *et al*. (1987) and deGroot-Hedlin & Constable (1990), the minimized objective function of the inverse process is given by

$$S(m) = (d_{\text{obs}} - g(m))^{\text{T}} W_d (d_{\text{obs}} - g(m)) + \alpha \cdot m^{\text{T}} Rm, \qquad (1)$$

where d_{obs} is the measured data, m is the model parameter, $g(m)$ is the calculated data by forward modelling, W_d is the data error weighting matrix and R is a roughness operator matrix. The smoothness factor α, which adjusts the amount of model roughness imposed during the inverse process, is determined with the method proposed by LaBrecque *et al*. (1996). The inverse and forward modelling also features a topography correction, which we applied with the DTM data collected after Typhoon Morakot.

RESULTS

2-D resistivity profiles

For all pole–pole measurements collected in the Siaolin area, the maximum standard deviation obtained by repeated measurements of apparent resistivity, which we call repetition error, are less than 2.6 per cent with a mean of 0.9 per cent for all survey lines. We are aware that LaBrecque *et al*. (1996) as well as Dahlin & Zhou (2004) noted that the repetition error alone may underestimate the noise level of resistivity measurements and suggested reciprocal measurements instead. Yet, due to limited time and budget, we did not collect any reciprocal measurements for a more detailed noise inspection. However, the repetition error provides us some valuable information in terms of data quality and remains within the error range suggested by Dahlin (1996). Honouring stationary conditions in terms of comparable error levels for the inverse solutions, the mean value was then taken as global data error weighting for all our inverse modellings. The resistivity inversions in general achieved the optimal estimations within five iterations and with the root mean square (rms) error of less than 3 per cent. In terms of the discussion before, this means that we slightly underestimated the data error level, but to an acceptable degree. With regard to the fact, that excavations are prohibitive in this area, we also used the DTMs from digital aerial images taken before and after Typhoon Morakot to help examine the inverted results. Fig. 3 is an overview of the results from the inverted-resistivity images of the electrical-resistivity imaging surveys along the networked lines in the Siaolin area. The topography before Typhoon Morakot is illustrated in Fig. 3 to provide a reference surface for the interpretation of resistivity results. Fig. 4 shows zoom-in inverted-resistivity images of selected NW–SE survey lines from A15 to A01, and Fig. 5 shows the images of NE–SW lines from NS0 to NS200.

Based on the geology records, the Yenshuikeng Shale was under most of the old ground surface and cropped out at locations in the river channels. The resistivity results illustrated in Figs 4 and 5 also show that an extended conductive basement with a resistivity of less than 25 Ω m is located below the level of the old river channel (note that the river channel changed after Typhoon Morakot) and is approximately 10–25 m deep with respect to the actual ground surface. Because the Yenshuikeng Shale is covered by fluvial sediments and only cropped out in the river channel before Typhoon Morakot, we concluded that the conductive basement that underlies the old fluvial sediments is most likely the Yenshuikeng Shale. Note that in Fig. 4, the conductive basement of Yenshuikeng Shale seems to disappear between −480 m and −600 m, and a relatively resistive layer (with resistivities over 120 Ω m) is observable at the same depth in profile A03 (the longest survey line). Having observed that the Tangenshan Sandstone slope was cropping out at approximately 50 m from the end of the A03 survey line, we concluded that this body (which is relatively resistive compared to the rest of the basement) may suggest the presence of the Tangenshan Sandstone.

Above the old ground surface, the overlaid sediments induced by the Siaolin landslide event are composed of resistive materials with resistivities of higher than 50 Ω m. In Figs 4 and 5, we found that the thickness of the debris-flow sediments is approximately 3–15 m on average and appears to become thicker from profile A01 toward A15. We also observed that sporadic regions with resistivities of less than 20 Ω m were located in the newly accumulated sediments shown in Fig. 3 (indicated by white arrows). These resistivity-anomalous regions may indicate the locations of buried anthropogenic constructs within the debris-flow sediments.

The old fluvial sediments may have been left between the debris-flow sediments and the Yenshuikeng Shale basement after Typhoon Morakot; however, because the smoothing approach was implemented in the inversion algorithm, it is difficult to clearly identify the upper and lower boundaries of the old layer with only resistivity images.

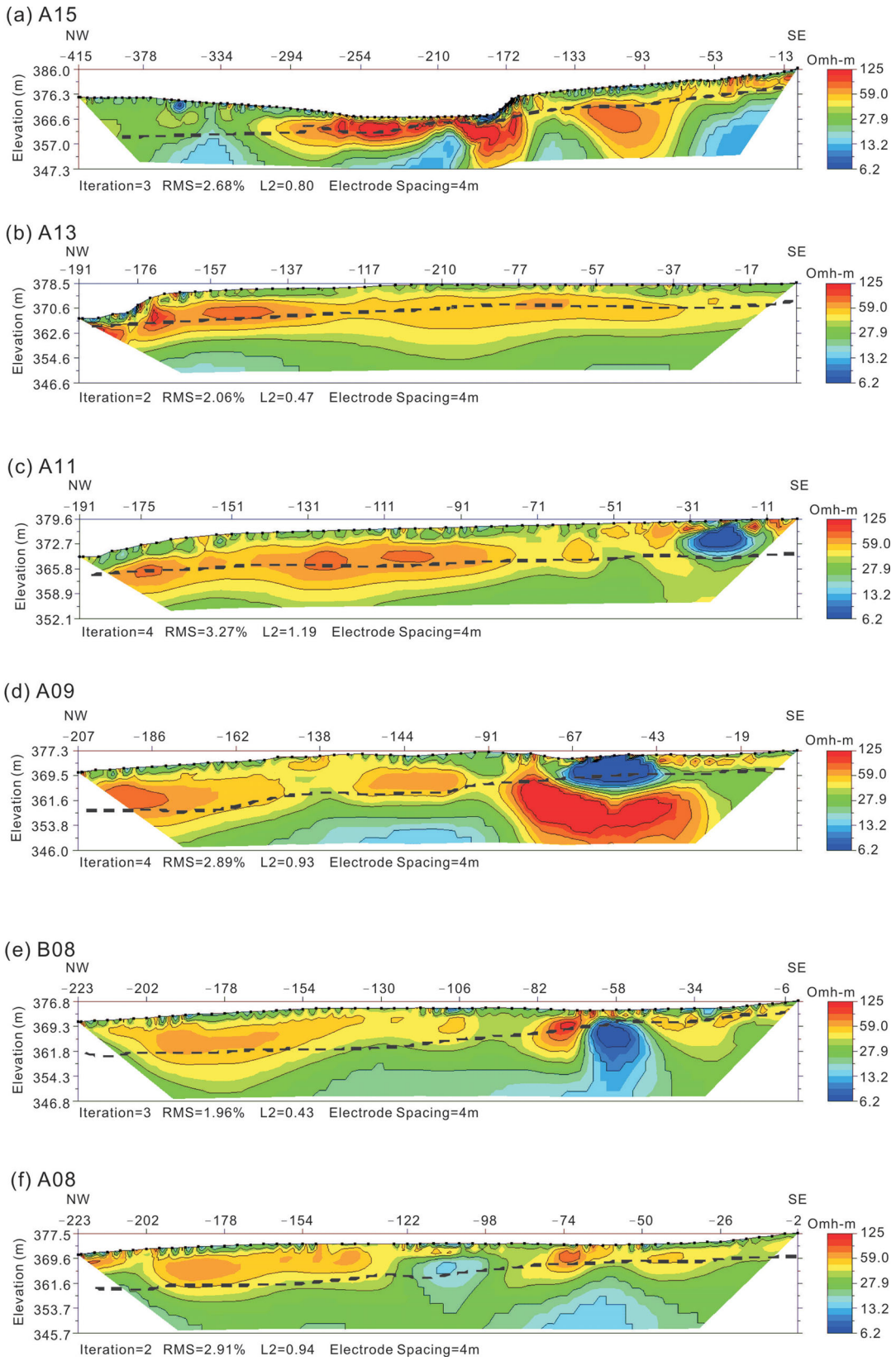

Figure 4. The inverted resistivity images of the survey lines in the NW–SE direction: (a) A15, (b) A13, (c) A11, (d) A09, (e) B08, (f) A08, (g) B07, (h) A07, (i) A06, (j) B05, (k) A03 and (l) A01. Dashed lines indicate the pre-Morakot ground surface. The horizontal distances are the distances in meters from the starting electrodes on line NS00. Negative signs symbolize the westbound orientation. L2-norm of iterative difference in model parameters is also shown to indicate the convergence of inversion.

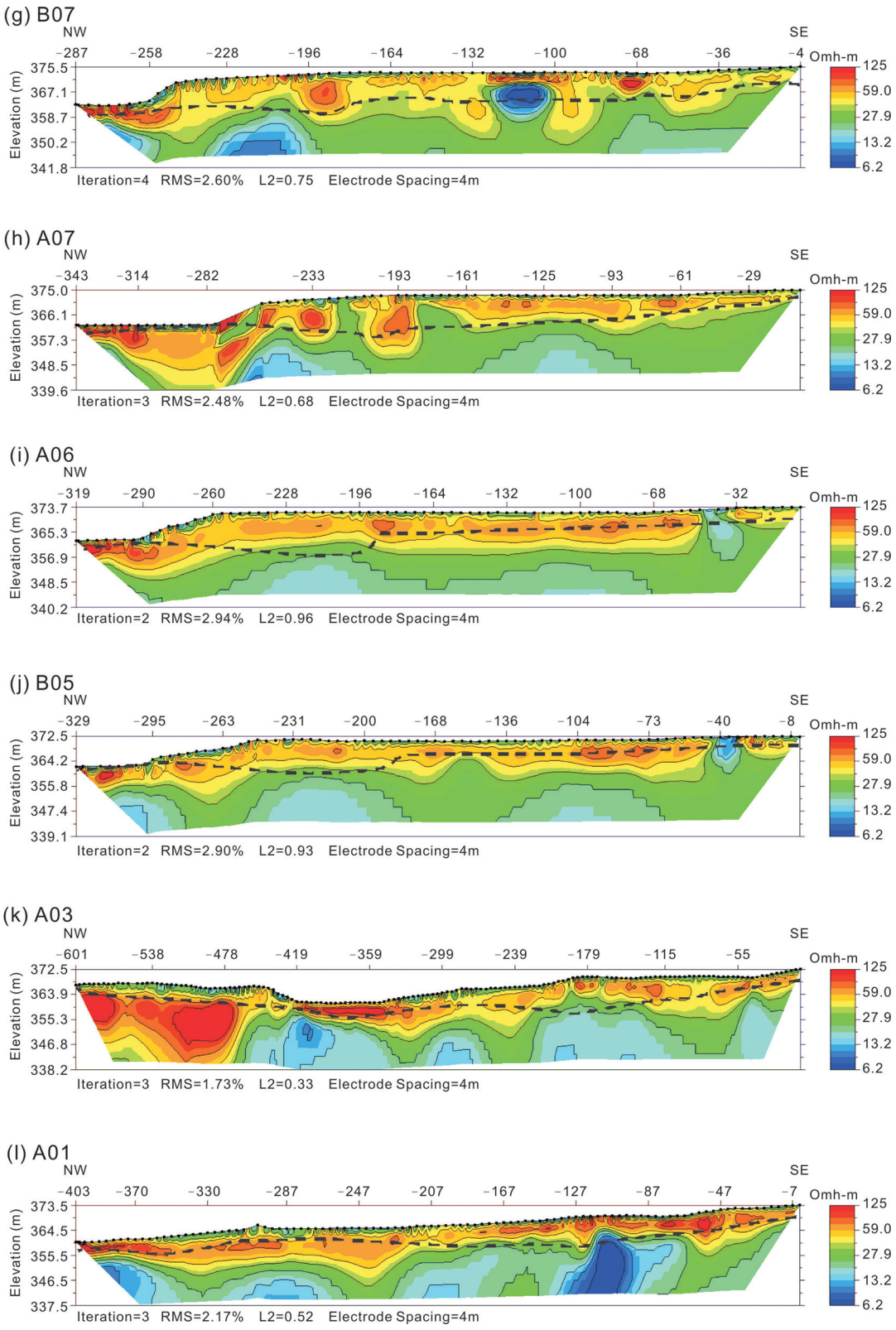

Figure 4. (*Continued*.)

Resistivity structures within the debris-flow sediments

From the resistivity images, we found that the newly accumulated sediments are below depths of 3–15 m relative to the current ground surface and that some resistivity anomalies indicate possible anthropogenic constructs inside them. For instance, a distinctive conductive region with resistivities of less than 25 Ω m was found near the surface in lines A09 and A11 between 40 and 70 m and between 10 and 40 m, respectively, from the starting electrode on NS00 (Fig. 4). To show the spatial relationships between these anomalies

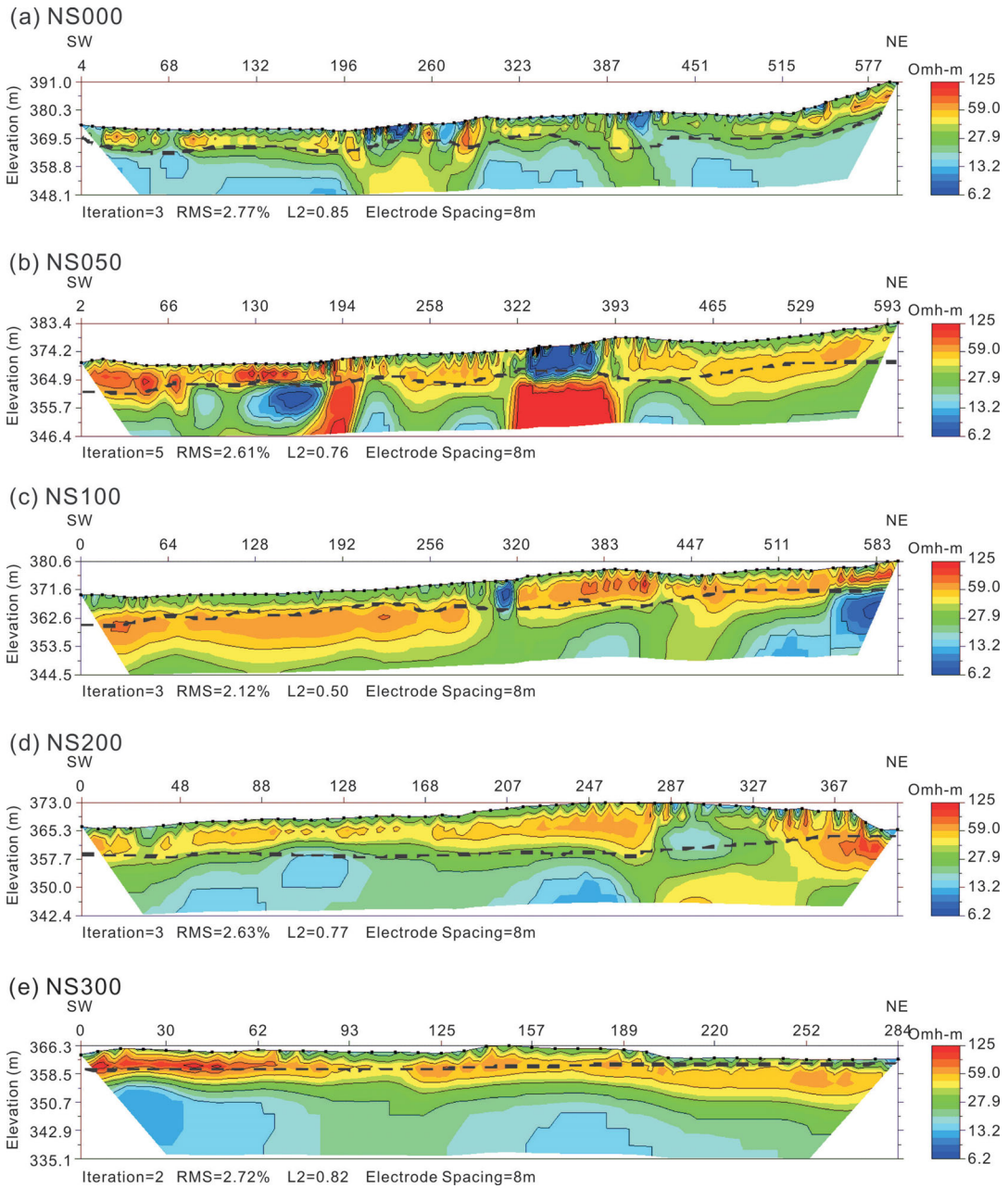

Figure 5. The inverted resistivity images of the survey lines in the NE–SW direction: (a) NS00, (b) NS050, (c) NS100, (d) NS200 and (e) NS300. Dashed lines indicate the old ground surface before Typhoon Morakot. The *x*-coordinate shows the distance in meters from the reference starting line. Positive signs symbolize the northbound orientation.

and the old landscape, we interpolated the resistivity values with inverse distance weighting (Shepard 1968) and plotted the interpolated resistivity values at a depth range of 8 ($\pm$ 1) m within the area enclosed by A01, A15, NS00 and NS200. We then compared it with the pre-Morakot map of Siaolin village (Fig. 6). The resistivity cross-section at 8-m depth coincides with the bottom of the identified debris flow in this region.

Fig. 6 shows that in some locations, the resistive and conductive anomalies can be correlated with pre-Morakot landscape features (such as roads and houses). Because the houses and buildings in the Siaolin area were mostly made of steel roofs and pillars with concrete walls, we can conclude that these anomalies represent the relics of anthropogenic constructs. The matching of the resistivity anomalies and the landscape locations suggests that we have detected some buried anthropogenic structures that remained at their original locations. On the other hand, Fig. 6 presents no anomalies in the northern part of the village where many houses were located before the typhoon. The absence of resistivity anomalies implies that the anthropogenic structures in this area may have been destroyed and completely washed away, or that the anthropogenic structures were buried at over the maximum exploration depths available to the instruments. From the geodetic measurements (e.g. Lee *et al*. 2009; Tang *et al*. 2009), we found that the old ground surface was located at the depth around 8–15 m in this region and should be detected with the resistivity exploration. As a result, we concluded that the anthropogenic constructs in the northern part of the village were most likely destroyed and transported away during Typhoon Morakot.

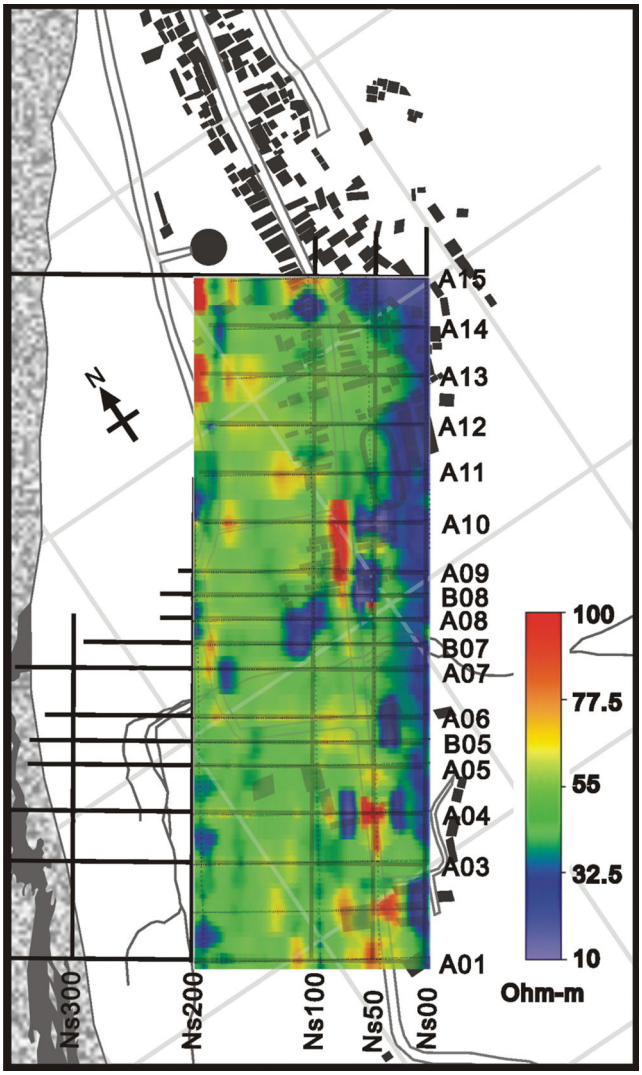

Figure 6. A comparison between the resistivity (in Ω m) cross-section at a depth of 8 m and the map of anthropogenic constructs in Siaolin village.

A comparison between the results of magnetic surveys, HLEM surveys and resistivity analyses

To further examine the resistivity anomalies induced by anthropogenic constructions, magnetic surveys and HLEM surveys were conducted in the Siaolin area. The magnetic surveys were conducted using a portable magnetometer at 1.22 or 1.82 m above the ground and recorded the total-field magnetic data (Doo *et al*. 2011). Portable proton precession magnetometers (Geometrics model G-856, with a sensitivity of 0.1 nT) were used in the magnetic surveys. The HLEM surveys were conducted with the CMD electromagnetic-conductivity meter (manufactured by GF instruments, s.r.o., Czech Republic), which provides the inphase and quadrature components of the secondary-to-primary field ratios. The device provides directly apparent conductivity at low induction numbers (McNeill 1980; Reynolds 1997).

Fig. 7 presents images of the magnetic anomalies and the HLEM apparent conductivities plotted on the pre-Morakot map of Siaolin village. The magnetic images (Fig. 7a) indicate clearly, that high positive/negative magnetic anomalies south of the red dashed line are consistent with the locations of buildings. It should be noted that few magnetic anomalies are found north of the dashed line in Fig. 7(a). Fig. 7(b) presents apparent conductivity obtained from the HLEM surveys. Similar to the magnetic anomalies, regions with conductivities greater than 45 mS m^{-1} in the HLEM image can be well correlated to the locations of buildings south of the red dashed line. Again, no anomalies with conductivities greater than 45 mS m^{-1} can be identified north of the dashed line in Fig. 7(b). Visually compared with the resistivity slice in Fig. 6, those magnetic anomalous and high conductive (greater than 45 mS m^{-1}) regions are in good agreement with regions that show resistivity values of less than 25 Ω m in Fig. 6. However, the HLEM results show no correlation between the regions of low conductivity and the regions with resistivity values of greater than 65 Ω m. This is likely because the HLEM method is much more sensitive to conductive bodies and near-surface structures (within a depth of 4–6 m). In addition, because some anthropogenic constructs might be buried at depths over the exploration capabilities of the HLEM survey, it is reasonable to observe that some conductive targets that appear in the resistivity image do not always show strong responses in the HLEM image.

A comparison between seismic-refraction and resistivity results

Because no excavations are allowed in the Siaolin area, the seismic refraction surveys were also carried out to reveal additional and complementary subsurface information. The seismic refraction surveys were conducted along the A03, A15 and NS50 lines to examine the layer boundaries, which were drawn from the resistivity results along the selected vertical cross-sections. For the surveys, we utilized the Geometrics StrataVisor NZ and Geode systems and 96 geophones registering 100 Hz with a spatial separation of 2 m. Energy sources were provided using a JMS-MINI 65 Impactor blowing at every 6 m along the survey line. The seismic-refraction measurements were processed with traditional plus–minus methods (Hagedoorn 1959). The calculated velocity profiles of the seismic-refraction surveys in Fig. 8 indicate three layers with distinct different velocities. These are: (1) the rock basement with a velocity of approximately 2800 m s^{-1} at depths between 15 m and 25 m; (2) the old fluvial sediments with a velocity of 1100 m s^{-1} at depths between 6 and 20 m and (3) the uppermost unconsolidated sediments with velocities of 300–400 m s^{-1} and above depths of 6–10 m.

In general, the layout of the velocity layers from the seismic-refraction surveys is in agreement with regions of similar resistivity values. In A03, we found that the basement of the westernmost 120 m is a very resistive body (Fig. 4k). The seismic profile shows that the velocity of materials at the basement level changes from 2800 m s^{-1} to 1600 m s^{-1} at the same location. This finding is consistent with the resistivity anomaly of the basement that is found at the same location, which indicates the presence of the Tangenshan Sandstone in the rock basement.

In A15, the sediments above the old ground surface in the westernmost 90 m are comprised of deposits with resistivity values between 25 and 45 Ω m. These values are less than the average resistivity of debris-flow sediments contributed from the eastern hills. With the exception of the uppermost loose sediments that have a very low velocity of 300 m s^{-1}, the velocity of the debris-flow sediments is approximately 770 m s^{-1} on the western bank of the river and is approximately 1100 m s^{-1} on the eastern bank (above the pre-Morakot ground surface at A15). This finding is again consistent with the resistivity results and shows two very different compositions in the debris-flow sediments in A15.

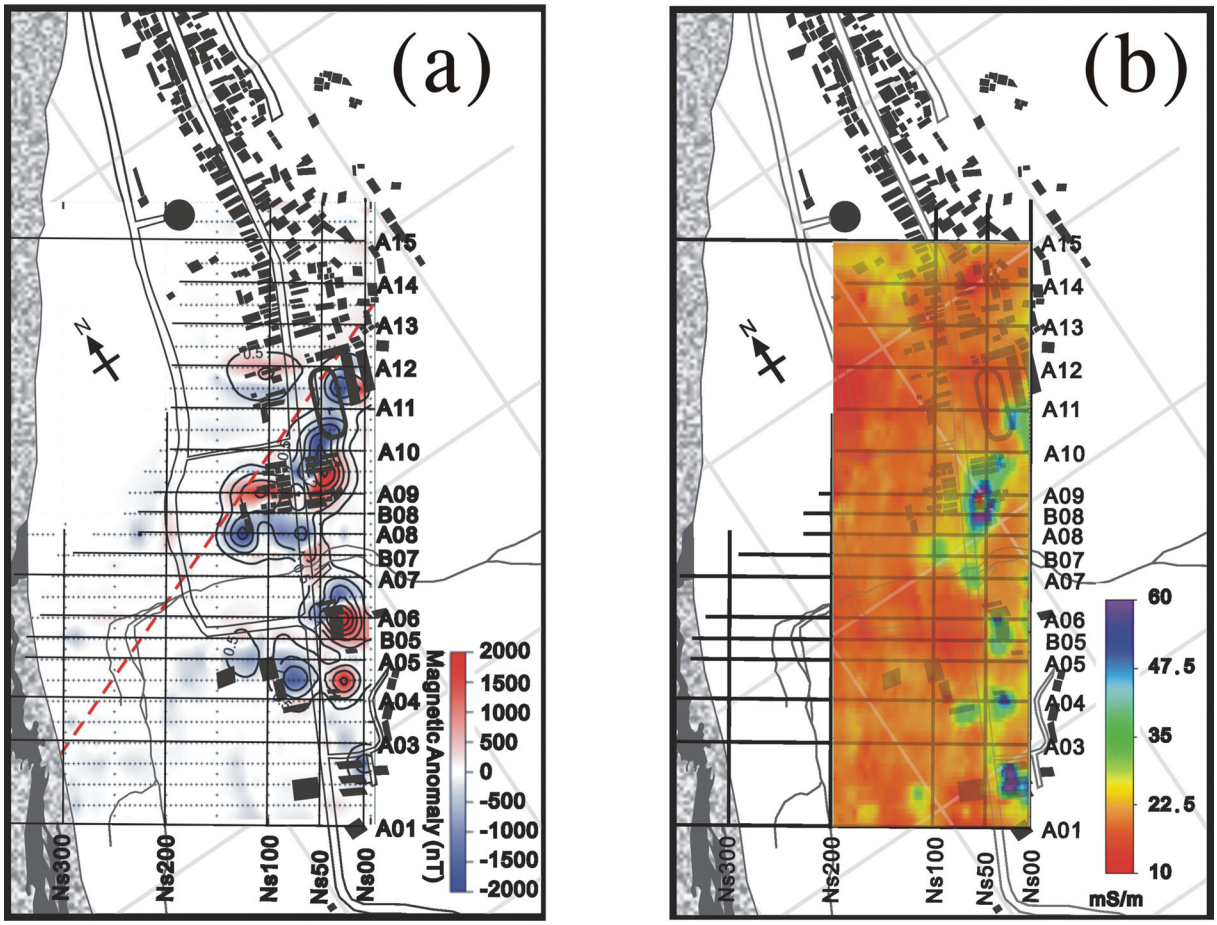

Figure 7. (a) A comparison between the magnetic-anomaly (in nT) image and the map of anthropogenic constructs in the Siaolin survey area. (b) A comparison between the HLEM apparent conductivity (in mS m^{-1}) and the map of anthropogenic constructs in the Siaolin survey area.

DISCUSSION

Resistivity resolutions for depths of debris-flow sediments

Because smoothness constraints and regularization techniques are applied in the data inversion algorithms, a question that is often asked is how effective the inverted-resistivity results are for providing depth estimations for the debris-flow sediments. Dahlin & Zhou (2004) utilized synthetic models to examine the resolutions and sensitivities of different arrays. To examine the resolutions of the resistivity surveys with the same electrode configurations utilized in the Siaolin field surveys, we built several geological models based on the exploration results in the Siaolin area. The models were designed to have three horizontal layers including: (1) the uppermost debris-flow sediments with a resistivity of 70 Ω m; (2) the middle compacted 'old' fluvial sediments with a resistivity of 30 Ω m and (3) the conductive basement that represents the Yenshuikeng Shale with a resistivity of 10 Ω m (Fig. 9a). Pole–pole arrays were simulated using 64 electrodes with a separation of 1 m, which was the single roll-along measuring configuration utilized in the Siaolin area. Every 2-D forward model has dimensions of 64 m long and 40 m deep, and the grid spacing was 0.5 m in the horizontal direction with an increasing spacing factor of 1.1 from 0.5 m in the vertical direction. We used the EarthImager^{TM} 2-D software for the forward-modelling tests.

Here, we focused on the issue of the resolution capabilities of the resistivity surveys for detecting the bottom of the debris-flow sediments located at different depths. Hence, in the different models we give several different depths (e.g., 3.6 m, 5.4 m, 8 m, 10 m and 13.1 m) for the debris-flow bottoms while the top surfaces of the conductive shale basements are fixed at a depth of 17 m. To test the sensitivity of inversion results to different inversion regularizations, we furthermore adopted three different schemes for the inversion of synthetic models. The inversion schemes (AGI 2009) include (i) the smooth inversion, which the object function is eq. (1), (ii) the damped least-square (DLS) inversion, which the object function is eq. (1) with smoothness factor α of zero and (iii) the robust inversion by minimizing the L1 norm. The object functions were solved with the conjugated gradient method. Fig. 9(b) shows an example of a synthetic pseudo-section with the debris-flow bottom at 8-m depth and the inverted results of the synthetic data with the smooth inversion method. Fig. 9(c) is a comparison between the inverted results with different inversion methods and the true model mentioned in Fig. 9(b). If we adopt a mean resistivity value that is between the values for the debris-flow and fluvial sediments (i.e. 45 Ω m) as an indicator to show the bottoms of the debris-flow sediments, we find depth estimation errors within 1 m for the models with debris-flow bottoms at less than 8 m (Fig. 9d) for all inversion methods. Within a depth of 8 m, the smooth inversion, the DLS and robust methods give similar estimations. However, if the depths of debris-flow sediments are increased to over 10 m, the

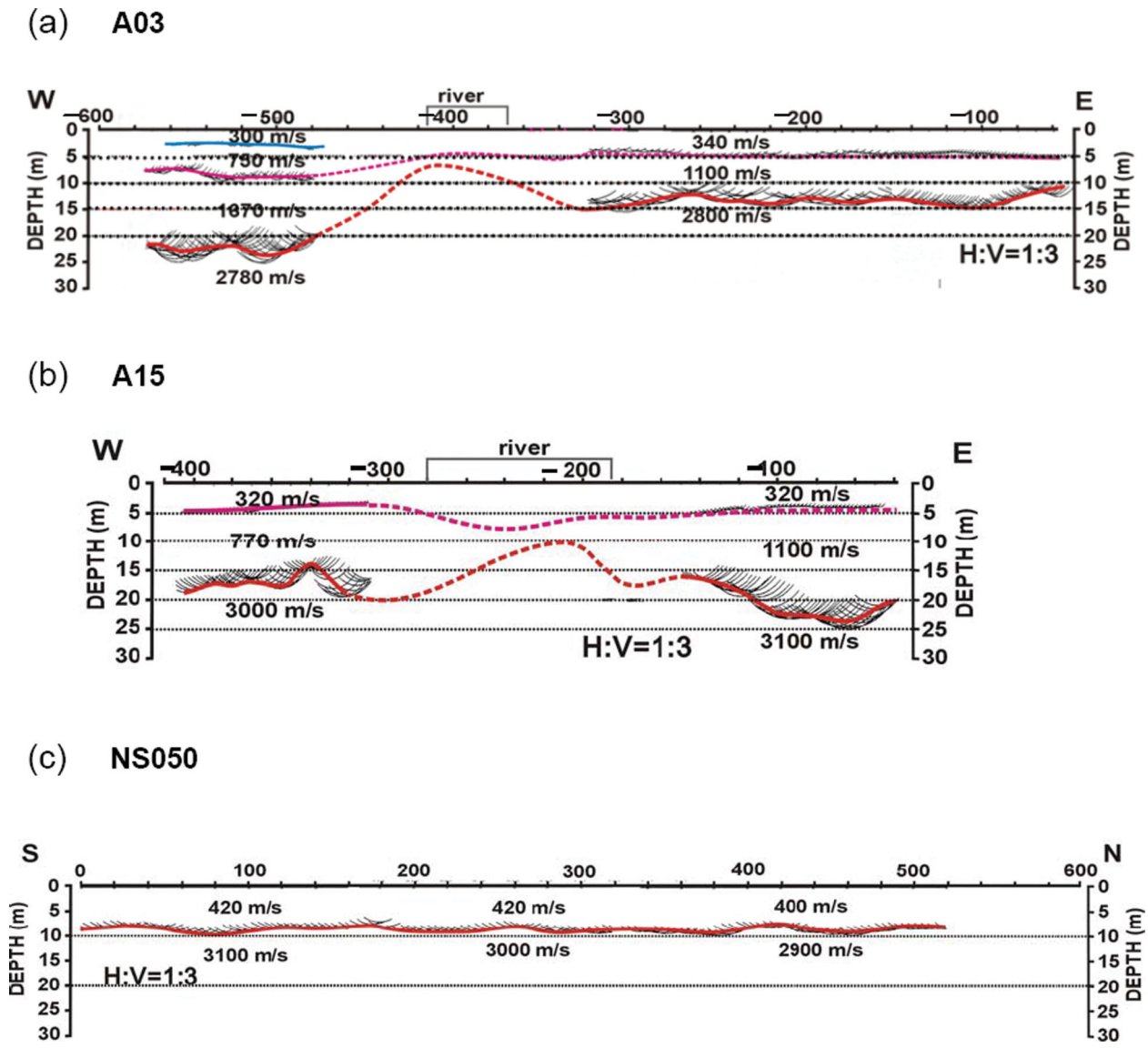

Figure 8. The resistivity results and the interpretations of the seismic refraction surveys of (a) line A03, (b) line A15 and (c) line NS50. The bottom of the debris flows and the top surface of the bedrock (from calculated velocity profiles) are delineated in pink and red lines, respectively. H : V = 1 : 3 means that the vertical scale is exaggerated three times the horizontal scale.

estimation with the smooth inversion method is worst than the DLS and robust methods. As the depths are greater than 12 m, the depths of debris flow will be underestimated with either one of the smooth inversion, DLS, or robust methods if 45 Ω m is used as an indicator. Therefore, care should be taken when using a fixed resistivity value for quantitatively delineating the lateral changes of a layer boundary if the boundary varies over a certain depth.

Resistivity results and the debris-flow distribution

The resistivity data showed that the newly accumulated debris-flow sediments generally exhibit resistivities greater than 45 Ω m and that the bottom debris-flow sediment level is at depths above 8–10 m. However, we also found that the bottom depths of the debris-flow sediments do not always coincide with the corresponding levels of the pre-Morakot ground surfaces. Some resistive and conductive anomalies are even below the old ground surfaces. For instance, the anomalous regions (with resistivities of less than 25 Ω m and greater than 65 Ω m) are below the line of the old ground surface (between 0 and 200 m in NS50; see Fig. 5b). The inconsistency between the resistivity results and the old ground surface may imply that as the debris flowed through the area, it undercut the old ground surface in certain places. Therefore, we tried to illustrate the areas with basal erosion and the areas without basal erosion to determine whether or not any spatial relationship exists between the distribution geometry and the geophysical results that we gathered.

In Fig. 10(a), we illustrate three basal erosion areas (C1, C2 and C3) where the bottom depths of the debris flow (judged according to the resistivity results) were found below the old ground surface. On the other hand, P1 indicates the area where the bottom of the debris flow is at the same level as (or above) the pre-Morakot ground surface. C1 is the area where some houses should be located but no resistivity anomalies were identified. P1 is the area where we found many conductive and resistive anomalies including responses from anthropogenic structures and the aforementioned thoroughfare. In area C2, we found some conductive and resistive anomalies along

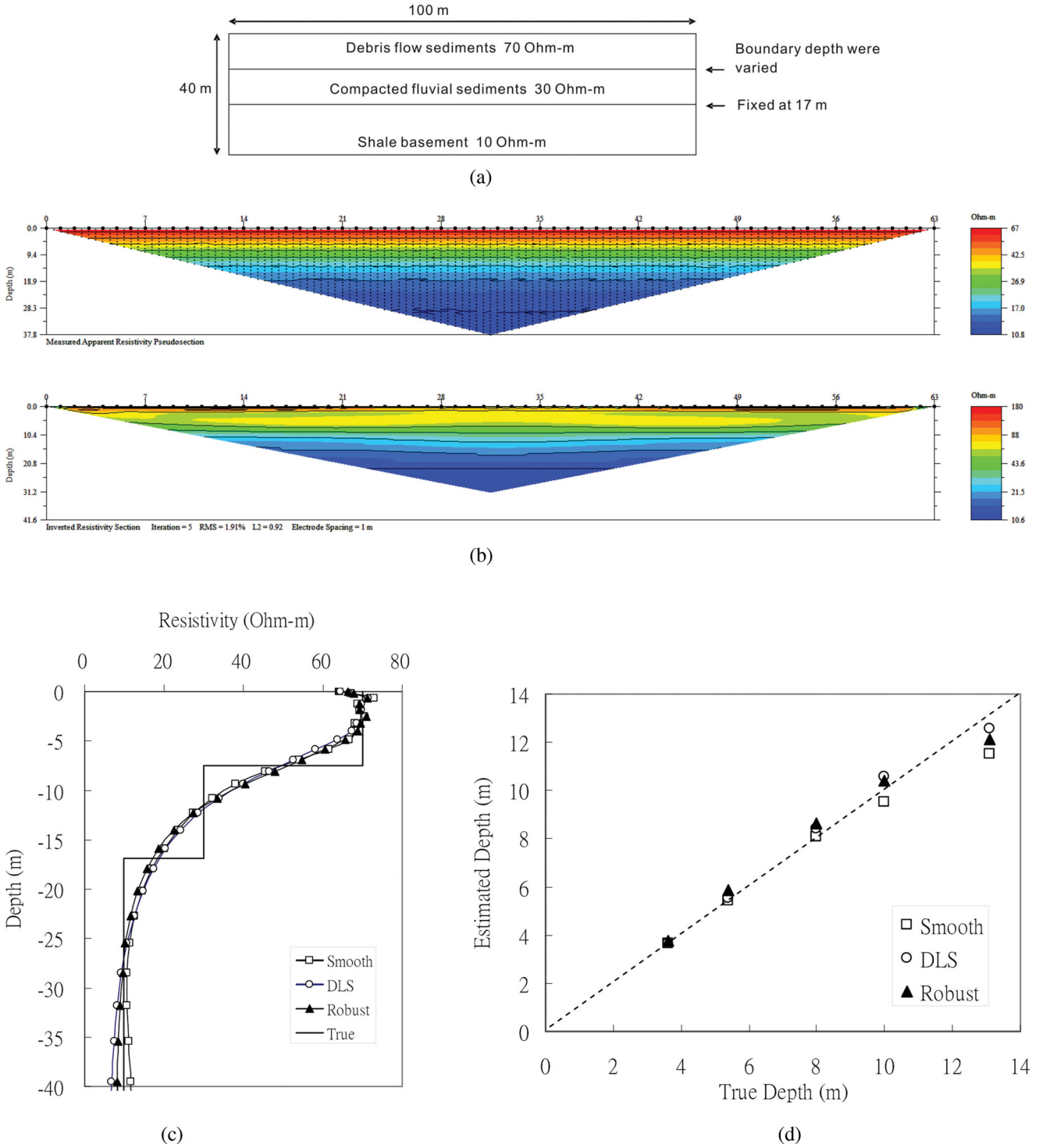

Figure 9. (a) The geological model for the resistivity-forward simulations. (b) An example of a synthetic pseudo-section with the debris-flow bottom at 8 m depth and the inverted result of the synthetic data. (c) The two graphs show examples of the inverted resistivity results (in solid lines) and the true model (in dash lines) in different forward simulations. (d) A comparison between the estimated depth (judged using a resistivity value of 45 Ω m) and the true depth of the debris-flow sediments.

the highway, and the locations of the anomalies are slightly offset from this anthropogenic structure's original location. It seems that between C1, C2 and C3 there existed a 'piling' area (i.e. P1) where no basal erosion occurred.

Fig. 10(b) compares the basal erosion and piling areas on a map that identifies the differences between the new and the old ground-surface levels in the study area. The piling area P1 (between C1, C2 and C3) is consistent with the regions that show accumulated sediments thicker than 8 m. In addition, this piling area (P1) appears to have a fan shape that surrounds area C2. The distribution of area C2 also agrees well with the thickness contours of accumulated sediment from the collapsed high ground to the east. The geometries

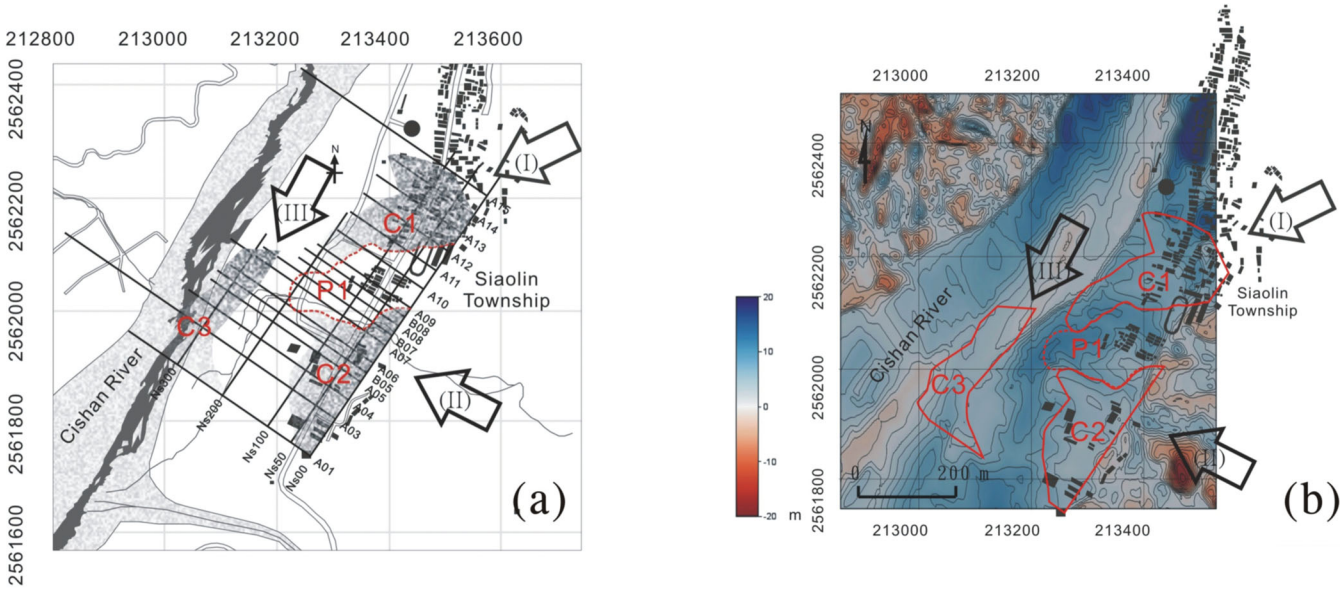

Figure 10. (a) The distribution of the basal erosion regions and the piling region in the study area. (b) A comparison of elevation differences between the current ground surface and the old ground surface (in blue-red scale with contours) and the locations of basal erosion regions. C1, C2, C3 indicate the areas eroded by the debris flow while P1 is the piling area. Arrows I, II and III indicate the three possible directions of debris flow from their different sources based on the testimonies of surviving witnesses in the Siaolin area.

of C2 and P1 suggest that the sediment most likely constitutes a small colluvial fan with debris flow from the collapsed high ground to the east. Although the elevation differences indicate that the debris-flow sediment is thicker at P1 than at C2, the actual thickness is approximately the same as in the areas of P1 and C2 if we take the basal erosion into account. Therefore, the debris-flow volume could be underestimated if only the DTM data are used for calculations comparing pre-Morakot and post-Morakot scenarios (e.g. Tang *et al*. 2009; Kuo *et al*. 2011). For the area bounded by A15, A01, NS00 and NS200, we estimated the volume of debris flow is about 727 000 m^3 from the DTM calculation and about 906 000 m^3 from the resistivity image estimation, respectively. The difference between the estimation from DTM and resistivity is 179 000 m^3, ∼24.5 per cent to the DTM-estimated volume of the debris flow in the encircled area.

In Fig. 10(b), C1 is next to the regions where the accumulated sediment is from the Xiandu Peak and is the thickest (over 20–30 m) in the study area. In addition, the area C3 is located along the zero-accumulation area, where the current ground surface is approximately the same as the old ground surface. The relationships linking C1, C2 and C3 to the DTMs of pre- and post-Morakot scenarios may suggest that the areas C1, C2 and C3 represent erosions of debris flow that pertain to different events (arrows in Fig. 10). The basal erosion area C1 is related to the debris-flow paths of the collapsing Xiandu Peak. C2 and the piling area are related to the colluvial fan originating from the collapsing high ground to the east of the village. It has been reported that the debris flow from Xiandu Peak blocked the Cishan River channel during Typhoon Morakot (Lee *et al*. 2009; Dong *et al*. 2011; Kuo *et al*. 2011). The collapse of the debris-flow dam (Dong *et al*. 2011; Li *et al*. 2011) caused the current channel to undercut the old ground surface. Because the area C3 is along the no-accumulation area (i.e. the area along the current channel that was formed later in the event), we conclude that C3 may be related to the later erosion phase induced by the collapsing of the debris-flow-blocked dam.

CONCLUSIONS

Using ERI surveys, we identified several layers of deposits in the Siaolin area including: (1) the basement of Yenshuikeng Shale at a depth of 20–25 m; (2) the newly accumulated debris-flow sediment with resistivity values of greater than 45 Ω m and reaching depths of 8–10 m and (3) the 'old' fluvial deposits between the basement and the newly accumulated debris flow. The results of seismic-refraction surveys also suggest similar three-layer structures along survey lines A03 and A15. The finding obtained from the seismic refraction survey is highly consistent with the ERI results and shows two very different compositions of the newly accumulated debris-flow sediments and the early fluvial deposits in the study area. Among the layers, we are most interested in the newly accumulated debris-flow sediments. We have illustrated the cross-section at a depth of 8 m relative to the current ground surface by interpolating the 2-D resistivity data with inverse-distance methods. The cross-section shows that the resistivity anomalies can be visually correlated to the pre-Morakot locations of houses, buildings and the village's major road. Because the magnetic and HLEM methods are sensitive to magnetic substances respectively conductive objects within 5–6 m of the surface, the results from the magnetic and HLEM surveys are consistent with the resistivity image at a depth of 8 m. After testing the resolution of different inversion regularizations of the ERI survey, we also confirm an estimation error within 1 m for the debris-flow bottoms at less than 8 m for all the smooth inversion, DLS and robust methods used. As the depths are greater than 12-m, the depths of debris-flow sediments will be underestimated with either one of the smooth inversion, DLS, or robust methods.

In addition, we found that the bottom of the debris-flow sediments (as identified from the resistivity results) can be found below the old ground surface in three areas: C1, C2 and C3. We also found that the anthropogenic structures remained near their original locations in areas P1 and C2. On the other hand, we detected no resistivity anomalies in area C1 where pre-Morakot houses once stood. The findings suggest that there was the basal erosion of debris-flow

sediments in areas C1, C2 and C3. Although the differences between the pre- and post-Morakot DTMs indicate that the debris-flow sediment is thicker at P1 than at C2, the actual thickness is approximately the same in these areas if we take the basal erosion surface into account. The previous DTM study showed that the eroded rock volume in the entire Siaolin area is about 25 673 847 m^3, and the volume of accumulated debris flow sediments is about 25 212 521 m^3 (Yeh *et al*. 2010). There are about 461 326 m^3 of debris-flow sediments washed away or unaccounted for in the area from the simple mass balance calculation. Note that the difference between the DTM- and resistivity-estimated volumes of debris-flow sediments is about 179 000 m^3 in the area surrounded by A15, A01, NS00 and NS200 lines. Therefore, one could underestimate the debris-flow volume if the DTMs were used for the pre- and post-Morakot calculations only.

Last, the relationships of C1, C2 and C3 to the debris flow suggest that these areas may represent basal erosion channels of debris flow from different events. In Fig. 10(b), arrows I, II and III indicate the three possible directions of debris flow from their different sources in the Siaolin area based on the testimonies of surviving witnesses (Lee *et al*. 2009; Dong *et al*. 2011) and simulations (Tang *et al*. 2009; Kuo *et al*. 2011; Li *et al*. 2011). The basal erosion area C1 is related to the debris-flow path of the collapsing Xiandu Peak. C2 and the piling area are related to the colluvial fan originating from the collapsing high ground to the east of the village. The area C3 may indicate a later erosion phase after the collapse of debris-flow sediments that blocked the riverbank, as C3 is located alongside the no-accumulation area.

ACKNOWLEDGMENTS

The authors dedicate this paper to the victims of the 2009 Siaolin catastrophe. This project was funded under grant NSC98–2745-M-008–013 of the National Science Council of Taiwan. Deepest appreciation is given to SeeHope Tech. & Eng. Ltd. Co., Taiwan for helping to collect the valuable magnetic data on Siaolin village. The comments and suggestions from Drs. Oliver Ritter, Hans-Balder Havenith and Roland Martin are much appreciated.

REFERENCES

AGI, 2009. *Instruction Manual for EarthImager^{TM} 2D Version 2.4.0*, Advanced Geosciences, Inc., Austin, Texas.

Bernstone, C., Dahlin, T. & Johnson, P., 1997. 3D visualization of a resistivity data set: an example from a sludge disposal site, *Symp. Appl. Geophy. Eng. Environ. Probl. Procs.,* 917–925.

Cassiani, G., Bruno, V., Villa, A., Fusi, N. & Binley, A., 2006. A saline trace test monitored via time-lapse surface electrical resistivity tomography, *J. appl. Geophys.,* **59,** 244–259.

Chen, C., 2010. Tragic moment of Shiaolin debris avalanche, Taiwan, reconstructed by near surface geophysical/geological and simulation evidence, *EOS, Trans. Am. geophys. Un.,* **91**(26), Abstract T42A-02.

Constable, S., R. Parker & C. Constable, 1987. Occam's Inversion: a practical inversion method for generating smooth models from EM sounding data, *Geophysics,* **52**, 289–300.

Corominas, J., 1995. Evidence of basal erosion and shearing as mechanisms contributing the development of lateral ridges in mudslides, flowslides and other flow-like gravitational movements, *Eng. Geol.,* **39,** 45–70.

Dahlin, T., 1996. 2D resistivity surveying for environmental and engineering application, *First Break,* **14,** 275–283.

Dahlin, T. & Loke, M. H., 1997. Quasi-3D resistivity imaging: mapping of 3D structures using two dimensional DC resistivity techniques, *Environ. Eng. Geophys. Assn. 3rd Mtg. Expended Abstracts*, 143–146.

Dahlin, T. & Zhou, B., 2004. A numerical comparison of 2D resistivity imaging with ten electrode arrays, *Geophys. Prospect.,* **52,** 379–398.

Daily, W. & Ramirez, A., 1992. Electrical resistivity tomography of vadose zone water movement, *Water Resour. Res.,* **28,** 1429–1442.

De Vita, P., Agrello, D. & Ambrosino, F., 2006. Landslide susceptibility assessment in ash-fall pyroclastic deposits surrounding Mount Somma-Vesuvius: Application of geophysical surveys for soil thickness mapping, *J. Appl. Geophys.,* **59,** 126–139.

Dong, J. J., Li, Y. S., Kuo, C. Y., Sung, R. T., Li, M. H., Lee, C. T., Chen, C. C. & Lee, W. R., 2011. The formation and breach of a short-lived landslide dam at Hsiaolin Village, Taiwan – Part I: Post-event reconstruction of dam geometry, *Eng. Geol.,* **123,** 40–59.

Doo, W. B., Hsu, S. K., Chen, C. C., Hsieh, H. H., Yeh, H. Y., Yen, H. Y., Chen, Y. G. & Chang, W. Y., 2011. Magnetic signature of Siaolin Village, southern Taiwan, after burial by a catastrophic landslide due to Typhoon Morakot, *Nat. Hazards Earth Syst. Sci.,* **11,** 759–764.

Friedel S., Thielen, A. & Springman, S. M., 2006. Investigation of a slope endangered by rainfall-induced landslides using 3D resistivity tomography and geotechnical testing, *J. Appl. Geophys.,* **60,** 100–114.

Green, A. G., Maurer, H., Spillmann, T., Heincke, B. & Willenberg, H., 2006. High-resolution geophysical techniques for improving hazard assessments of unstable rock slopes, *Leading Edge,* **25,** 311–316.

Griffith, D. H. & Barker, R. D., 1993. Two-dimensional resistivity imaging and modelling in areas of complex geology, *J. appl. Geophys.,* **29,** 211–226.

deGroot-Hedlin, C. & Constable, S. 1990. Occam's inversion to generate smooth, two-dimensional models from magnetotelluric data, *Geophysics,* **55,** 1613–1624.

Hagedoorn, J. G., 1959. The plus-minus method of interpreting seismic refraction sections, *Geophys. Prospect.,* **7,** 158–182.

Hsu, H. L., Yanites, B., Chen, C. C. & Chen, Y. G., 2010. Bedrock detection using 2D electrical resistivity imaging along the Peikang River, central Taiwan, *Geomorphology,* **114,** 406–414.

Labrecque, D. J., Miletto, M., Daily, D., Ramirez, A. & Owen, E., 1996. The effects of noises on Occam's inversion of resistivity tomography data, *Geophysics,* **61,** 538–548.

Lee, C. T., Dong, J. J. & Lin, M. L., 2009. Geological investigation on the catastrophic landslide in Siaolin Village, southern Taiwan, *Sino-Geotechnics,* **122,** 87–94 (in Chinese with English abstract).

Li, M. H., Sung, R. T., Dong, J. J., Lee, C. T. & Chen, C. C., 2011. The formation and breaching of a short-lived landslide dam at Hsiaolin Village, Taiwan – Part II: simulation of debris flow with landslide dam breach, *Eng. Geol.,* **123,** 60–71.

Kuo, C. Y., *et al*. 2011. The landslide stage of the Hsiaolin catastrophe: Simulation and validation, *J. geophys. Res.,* **116,** F04007, doi:10.1029/2010JF001921.

McNeill, J. D., 1980. *Electromagnetic Terrain Conductivity Measurement at Low Induction Numbers*, Technical Note TN-6, Geonics Ltd., Missisauga, Ontario.

Piegari, E., Cataudella, V., Di Maio, R., Milano, L., Nicodemi, M. & Soldovieri, M.G., 2009. Electrical resistivity tomography and statistical analysis in landslide modeling, *J. appl. Geophys.,* **68,** 151–158.

Reynolds, J. M., 1997. *An Introduction to Applied and Environmental Geophysics,* John Wiley & Sons Ltd, Malden, MA, 796 pp.

Shepard, D., 1968. A two-dimensional interpolation function for irregularly-spaced data, in *Proceedings of the 1968 ACM National Conference,* New York, NY, pp. 517–524.

Tang, C. L., Hu, J. C., Lo, C. M. & Lin, M. L., 2009. The catastrophic 1999 Tsaoling and 2009 Hsiaoling landslides: preliminary study from 3-D distinct element modeling, *Sino-Geotechnics,* **122,** 143–152 (in Chinese with English abstract).

Telford, W. M., Geldart, L. P., Sheriff, R. E. & Keys, D. A., 1986. *Applied Geophysics,* Cambridge University Press, London.

Yang, X., 1999. Stochastic inversion of 3-D ERT data. *PhD thesis,* Univ. Arizona.

Yeh, K. S., Li, M. Y. & Wang, U. H., 2010. Applying digital aerial images in nature hazards mitigation in Taiwan, *J. Photogramm. Remote Sens.,* **15,** 123–140 (in Chinese with English abstract).